

One- and two-photon fluorescence resonance energy transfer microscopy to establish a clustered distribution of receptor-ligand complexes in endocytic membranes

Horst Wallrabe

University of Virginia
Department of Biology
Gilmer Hall, 057
Charlottesville, Virginia 22904

Michael Stanley

Chroma Technology Corporation
74 Cotton Mill Hill
Brattleboro, Vermont 05301

Ammasi Periasamy

University of Virginia
Department of Biology
W. M. Keck Center for Cellular Imaging
Gilmer Hall, 064
Charlottesville, Virginia 22904

Margarida Barroso

University of Virginia
Department of Biology
Gilmer Hall, 057
Charlottesville, Virginia 22904
E-mail: mmb8n@virginia.edu

Abstract. One- and two-photon fluorescence resonance energy transfer (FRET) microscopy, using different bandwidth emission filters and a novel spectral spillover correction algorithm (PFRET algorithm), provides the basis for a quantitative approach to measure receptor clustering in endocytic membranes. Emission filters with wider bandwidth allow for an increased FRET signal and corresponding spillover. Treatment with the PFRET correction algorithm results in increasing correction levels and comparable energy transfer efficiency (E%) values, thus validating our algorithm-based approach. The relationship between E% and acceptor and donor levels and donor:acceptor (D:A) ratio is used to characterize the distribution of receptor-ligand complexes in endocytic membranes. In addition to the standard test for clustering (E%'s independence from acceptor levels), we describe a second parameter: the negative dependence of E% on increasing donor levels and D:A ratio. A donor geometric exclusion hypothesis is proposed to explain this phenomenon. One- and two-photon FRET microscopy assays show that polymeric IgA-receptor-ligand complexes are organized in clusters within apical endocytic membranes of polarized Madin-Darby canine kidney cells. © 2003 Society of Photo-Optical Instrumentation Engineers. [DOI: 10.1117/1.1584444]

Keywords: MDCK cells; polymeric IgA receptors; energy transfer efficiency; FRET; clustering; one- and two-photon microscopy.

Paper MM-16 received Apr. 6, 2003; revised manuscript received Apr. 18, 2003; accepted for publication Apr. 21, 2003.

1 Introduction

Fluorescence resonance energy transfer (FRET), and in particular energy transfer efficiency (E%), represents a powerful tool to investigate and quantitative biological processes, including protein-protein interactions and co-localization.^{1–6} For the energy transfer to take place, four conditions have to be met. First, there has to be significant overlap between the donor fluorophore emission spectra and the acceptor fluorophore excitation spectra (Fig. 1). Second, the average distance between donor and acceptor fluorophore molecules should be around 10 to 100 Å. Third, there has to be optimal dipole-dipole orientation of donor and acceptor molecules. Fourth, the donor has to exhibit sufficient quantum yield. Since energy transfer itself is a dipole-dipole interaction, no photons are transferred.

There are certain shortcomings of FRET microscopy, which need to be addressed when attempting quantitative approaches. Because of the spectral overlap, necessary for FRET to occur in the first place, the signal is contaminated with donor crosstalk and acceptor bleed-through (Fig. 1). The overlap between the donor and acceptor emission spectra results in donor crosstalk. Acceptor bleed-through occurs when the donor excitation wavelength excites part of the absorption spectrum of the acceptor. Emission filters with different bandwidths have been used to remove donor crosstalk and accep-

tor bleed-through contamination, provided this does not cause a major reduction in the FRET signal. Different algorithm-based correction methodologies exist and have been reviewed previously.^{7–11} Recently, we have developed a highly sensitive algorithm based on single label reference specimens, which corrects the contaminated FRET signal in a pixel-by-pixel manner (PFRET algorithm).¹² This new correction method is favorable to obtain highly sensitive corrected FRET signals.¹² To verify the robustness of the algorithm, we have compared fluorescence data acquired with different emission filters, capturing different levels of FRET signals and corresponding spillover contamination, and found comparable energy efficiency transfer (E%) values using one-photon (1-P) and two-photon (2-P) microscopy.

In our biological system, we have internalized polymerized IgA-receptor (pIgA-R) ligands—labeled with Alexa488 and Cy3 fluorophores—from opposite plasma membranes in Madin-Darby canine kidney (MDCK) cells (Fig. 2), which are stably transfected with rabbit pIgA-R.¹³ Previously, we used confocal microscopy to show that basolaterally and apically internalized ligands co-localize in the apical endosome,¹³ which is found in the subapical region (Fig. 2). Although the apical endosome transport pathways have been described be-

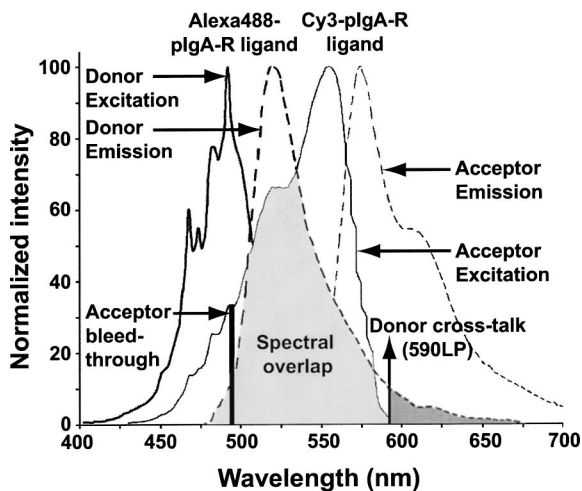


Fig. 1 Excitation and emission spectra of Alexa-488 and Cy3-labeled pIgA-R-ligand complexes. Significant spectral overlap (lighter shaded area) between donor (Alexa488) emission and acceptor (Cy3) excitation is essential for the occurrence of FRET. Acceptor bleed-through occurs when the donor excitation wavelength (488 nm) excites acceptor fluorophores leading to spillover contamination into the FRET signal in the acceptor channel (black vertical bar at 488 nm). Donor crosstalk occurs when the donor emission contaminates the FRET signal in the acceptor channel (darker shaded area to the right of 590 LP emission filter).

fore, the morphology of this apical endosome has not been fully characterized.^{13–16} Under normal physiological conditions (37 °C) these complexes are transported from the sub-apical region to the apical PM; under our internalization conditions (17 °C) both are retained in the subapical region due to a low-temperature exocytic block.^{13,17} It is important to note that receptor-ligand complexes internalized from opposite PM domains remain bound throughout transcytosis and recycling membrane trafficking pathways.¹³

The FRET assay uses the relationship of acceptor and donor fluorescence levels to $E\%$ to determine whether differently labeled receptor-ligand complexes are organized in a clustered or random distribution in apical endocytic membranes. As modeled previously, $E\%$ being independent of the acceptor is one indicator of a clustered distribution;¹⁸ another indicator shown here is the decreasing $E\%$ values with increasing donor levels and donor:acceptor (D:A) ratio.^{19,20} We call this phenomenon donor geometric exclusion, where increasing numbers of donors prevent other donors from interacting with a potential acceptor. The $E\%$ vs donor relationship is particularly valuable for our 2-P microscopy system, since the acceptor Cy3 is not excited at all by the 2-P donor wavelength and thus acceptor information is not collected.

The data presented here demonstrate comparable results using either 1-P or 2-P fluorescence microscopy to establish a clustered distribution of receptor-ligand complexes in endocytic membranes. Different bandwidth filters and a sensitive algorithm-based method have been used to correct FRET spillover contamination. Donor geometric exclusion phenomenon, which describes the $E\%$ decrease with increasing donor levels and D:A ratio, is used as another indicator of clustering that is particularly useful when acceptor data is not available as in 2-P microscopy.

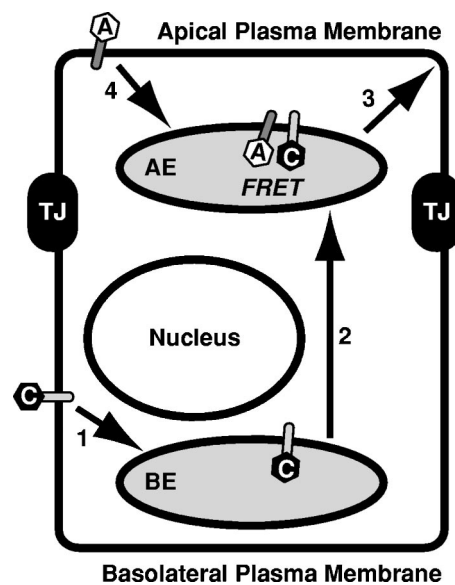


Fig. 2 Transcytotic and recycling pathways of pIgA-R ligands in polarized MDCK cells. Cy3- and Alexa488-labeled pIgA-R ligands are co-internalized from basolateral and apical PM domains, respectively. (1) Internalization and delivery to basolateral endocytic (BE) compartments; (2) transcytotic delivery to apical endocytic (AE) compartments; (3) delivery to apical PM from AE compartments; and (4) apical endocytosis and delivery to AE compartments. The black hexagon C is the basolaterally internalized Cy3-labeled pIgA-R ligand (acceptor) and the white hexagon A represents the apically internalized Alexa488-pIgA-R ligand (donor). Both complexes cross in the AE compartments and accumulate there upon internalization at 17 °C, which prevents transport to the apical PM. Images are collected at the apical cytoplasm (~3.5 μm below apical PM) to assay for FRET. Cell height is ~15 to 20 μm in our experimental conditions.

2 Materials and Methods

2.1 Spectral Analysis

Specific spectral analysis of protein-fluorophore conjugates used in our experiments was performed. First, 500 μl of 1 μM of pIgA-R ligands ($[\text{Fab}]_2$ pseudoligands against pIgA-R) conjugated to Alexa488 (Molecular Probes, Eugene, OR) or Cy3 (Amersham Life Science, Pittsburgh, PA) were prepared in PBS, as described previously.¹³ Luminescence intensity measurements to obtain the individual spectra were carried out using a Spex Fluorolog 2+2 spectrofluorimeter. All data were collected with right angle detection at room temperature ($22 \pm 2^\circ\text{C}$) in air-saturated solutions. Excitation and emission intensity data were evaluated at the maximum.

2.2 Growing MDCK Cells on Filter Insert

MDCK cells stably transfected with pIgA-R were grown to confluence in 100-mm cell culture dishes. After 4 days, the cells were trypsinized, centrifuged, and resuspended in DMEM/10% FBS/Pen-Strep.¹³ Then, 120 μl of the cell suspension was placed on top of an inverted Transwell Clear insert (Corning Costar, Cambridge, MA), i.e., on the outside of the membrane.¹⁴ After 4 h, the inserts are placed the normal way into multiwell dishes containing DMEM/10% FBS/Pen-Strep. After 3 days in culture these cells are fully polarized and are used immediately according to specific internalization protocols.¹³

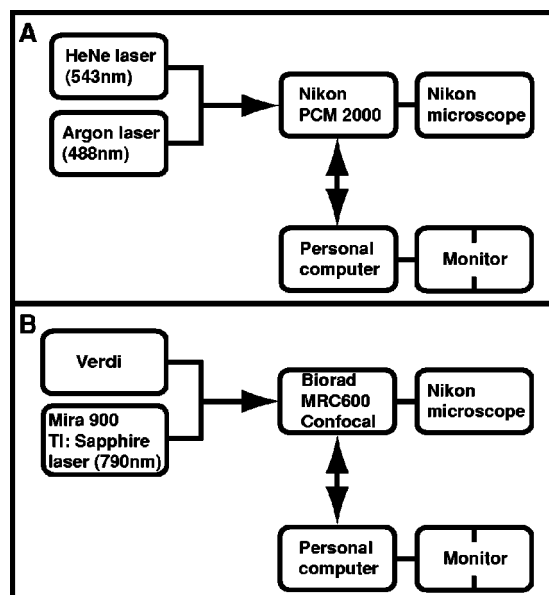


Fig. 3 1-P and 2-P microscopy systems. Schematic illustration of the (a) laser scanning confocal 1-P and (b) multi-photon 2-P excitation fluorescence microscopy systems integration.

2.3 Internalizing Fluorophore-Labeled Ligands

The inserts with polarized MDCK cells are washed with PBS and equilibrated with DMEM/HEPES/BSA at 17 °C. Next, 160 $\mu\text{g/ml}$ Alexa488- or Cy3-labeled pIgA-R ligands were co-internalized from apical and basolateral PM, respectively. Cells are incubated at 17 °C for 4 h to allow internalization of pIgA-R-ligand complexes into the subapical region by basolateral-to-apical transcytosis and apical endocytosis. At 17 °C, delivery to the apical PM is blocked and receptor-ligand complexes, co-internalized from opposite PM surfaces, localize predominantly in the apical endocytic compartment, which is located ~ 1 to 5 μm below the apical PM.¹³ Our images were collected 3.5 μm below the apical PM (Fig. 2; FRET). Then, the cells are washed with PBS to remove unbound ligands and immediately fixed with 4% paraformaldehyde/PBS.

Three different samples were used during our experiments: the double-labeled specimen, containing apically internalized Alexa488-pIgA-R-ligand complexes and basolaterally internalized Cy3-pIgA-R-ligand complexes, plus corresponding single-label reference samples containing either Alexa488 or Cy3, which were used to establish the contamination levels.

2.4 1-P and 2-P FRET Microscopy

For the 1-P data collection, we used a Nikon PCM 2000 laser scanning confocal microscope [Fig. 3(a)], equipped with a 60 \times water immersion lens (1.2 NA), argon (488 nm) and green HeNe (543 nm) lasers, and emission filters (515/50 nm and 590 nm LP for our standard experiments), respectively. For the experiments comparing different emission filters, we have used 580/20, 580/30, 580/40, 580/50, and 610/75, provided by Chroma Corp. (Brattleboro, VT), and our standard 590 LP. Simple PCI software (Compix, Cranberry Township, PA) was used to drive the hardware, image acquisition, and processing [Fig. 3(a)]. Bleaching is undetectable when the

argon laser is only used for one scan to collect the final image. PCM is set to collect data simultaneously in both channels at a 1024 \times 1024 pixel image.

For the 2P-FRET experiments we used a VERDI pumped turntable mounted titanium:sapphire laser, coupled to the laser port of a Biorad MRC600 (Biorad, Hercules, CA). The MRC600 scan head is coupled to a Nikon TE300 (Eclipse) epi-fluorescent microscope (Nikon, Melville, NY), linked to a personal computer and monitor [Fig. 3(b)]. For data collection, the same specimens were used as in the laser scanning confocal experiment. The objective was a 60 \times water immersion lens (1.2 NA), with the laser excitation wavelength at 790 nm and a 4.0 power level. We used this laser excitation wavelength to excite specifically the donor molecules. We used a 535/50-nm donor emission filter and our standard 610/60-nm acceptor filter, plus, for comparative measurements, the above-mentioned 580/20-30 series. Fluorescence levels are presented simultaneously on a split screen, one representing the donor channel and the other the acceptor channel.

2.5 Data Collection

For both 1-P and 2-P microscopy, the specimen is positioned in a small chamber created by a coverslip between two metal rings and filled with a small amount of PBS. This whole assembly is placed on the microscope stage. We first select an appropriate area of the specimen, check the cell height (15 to 20 μm), and set a focal plane of 3.5 μm below the apical PM. For 1-P this is done with only the green HeNe laser in operation, and for 2-P at 790 nm; in both cases in an area of the specimen that is not used later for image acquisition. Optimal PMT settings are established in the pre-image-acquisition phase.

2.5.1 1-P microscopy

With the zoom setting at 2.3 and without any image processing, a one-scan image of the double-labeled specimen is taken with only the Green HeNe laser/acceptor excitation (the argon laser is blocked). This is followed by a one-scan image with only the argon laser/donor excitation (green HeNe laser blocked). The single-labeled acceptor specimen follows the same protocol; the single-labeled donor specimen is only scanned with the argon laser, as we do not observe fluorescence when subjected to the acceptor excitation. Images of all three types of specimen are taken under the exact same conditions: 60 \times water immersion lens, PCM 1024 color, 2.3 zoom, and no processing.

2.5.2 2-P microscopy

With the zoom setting at 2.3, a one-scan image of the double-labeled specimen is taken at 790 nm and images are collected in both channels simultaneously. This is followed by imaging of the single-labeled donor specimen under identical conditions.

2.6 Post-Acquisition Data Generation and Analysis

2.6.1 Algorithm removes spillover contamination

As described in the introduction, there are two contaminants in the FRET signal: donor crosstalk and acceptor bleed-through. We have developed the PFRET algorithm, which re-

moves these contaminants pixel-by-pixel on the basis of matched fluorescence levels between the double-label specimen and a single-label reference specimen using seven images based on 1-P microscopy: two single-label donor reference images (donor excitation/donor channel and acceptor channel); two single-label acceptor reference images (donor and acceptor excitation, both in the acceptor channel); and three double-label images (donor excitation/donor and acceptor channel, acceptor excitation/acceptor channel).¹² For example, to remove the acceptor bleed-through, fluorescence levels are matched pixel by pixel between the double-label and single-label acceptor specimen, which were imaged under identical conditions. Those specific pixel location coordinates are recorded by the program and tracked to the same locations in the respective images taken at donor excitation in the acceptor channel (FRET channel). The fluorescence appearing here in the single-label specimen represents acceptor bleed-through and may be assumed to be identical in the double-label specimen at the same acceptor intensity levels, and is subsequently deducted pixel by pixel from the contaminated, uncorrected FRET (uFRET) signal. The donor crosstalk is removed analogously to finally achieve the precision FRET (PFRET) image.

For 2-P microscopy, the same algorithm-based program is used, except that only four images are necessary, since there is no acceptor bleed-through¹²: two double-label images (donor excitation in the donor and acceptor channel) and two single-label donor images (donor excitation in the donor and acceptor channel).

2.6.2 Calculating energy transfer efficiency (E%)

The calculation of E% is central to differentiating between random and clustered distribution of membrane-bound components as well as to estimate the distance between molecules.³ We have not considered the calculation of distance in our co-localization scenario, which by definition deals with variable distances. There are different ways to calculate E%,^{3,18} however, the principle is to establish the difference between the quenched and unquenched donor (uD) levels (=energy transfer) and relate that value to uD, which expresses as a percentage how much of the potential energy was transferred. With our algorithm-based method, PFRET represents the actual energy transfer, which we add to the quenched donor fluorescence, pixel-by-pixel, producing an uD value. This allows us to calculate E% ($=100 \times \text{PFRET} / \text{quenched donor} + \text{PFRET}$) and, together with the other double-label data, its relationship to acceptor and donor. Image processing and analysis for E% calculation was performed as described previously.^{12,19} Comparison between different images is possible since excitation efficiencies, quantum yields of fluorophore molecules, and detection efficiencies are assumed constant throughout our experiments.

3 Results

3.1 Spectral Overlap of Alexa488- and Cy3-labeled pIgA-R Ligands

For energy transfer to occur, the donor and acceptor fluorophores need to possess sufficient spectral overlap between their emission and excitation spectra, respectively. In our FRET experiments, Alexa488 acts as the donor and Cy3 as the

acceptor (Fig. 1). For this particular fluorophore pair the highest efficiency of energy transfer is at a distance of 67.5 Å, when 50% of excited donors are deactivated by FRET.⁴ Below and above 67.5 Å, FRET occurs at a reduced rate. To assess the extent of spectral overlap between Cy3 and Alexa488-pIgA-R ligands, a correct spectrogram for this fluorophore-protein pair was determined (Fig. 1). This fluorophore pair provides an excellent fit for FRET microscopy showing a strong spectral overlap. Unavoidably, background fluorescence, i.e., acceptor bleed-through and donor crosstalk, also occurs. When donor excitation takes place at 488 nm, some acceptor fluorophores will be excited due to the spectral overlap (acceptor bleed-through), thus contaminating the FRET signal (Fig. 1). Equally, that part of the donor emission spectrum that overlaps with the acceptor emission and is not curtailed by filters (donor cross-talk) will also add to the FRET spillover contamination (Fig. 1).

3.2 Algorithm-Based Correction Method for FRET

For biological systems where the fluorophore pairs are not always separated by a consistent distance and where FRET occurs over a wide range of fluorescence intensities at a membrane plane, the importance of a sensitive, finely tuned correction system cannot be overstressed. In the absence of reliable correction methods, small changes expressed in differential FRET signals may be misinterpreted, particularly where the FRET signal approaches the fluorescence level of the background contamination. Recently, the PFRET algorithm method was developed to correct the FRET spillover contamination in a pixel-by-pixel manner.¹²

The PFRET correction algorithm for 1-P microscopy requires seven images to correct the double-label 1-P FRET images, as described previously.¹² Those include images of single-label reference donor and acceptor, as well as double-labeled specimens with comparable fluorescence ranges taken under identical imaging conditions (data not shown). Applying the algorithm with different reference specimens produces near-identical results, indicating that different single-label controls do not change the correction level (data not shown).

1-P images showing a two-dimensional Z-section (i.e., in the *xy* plane) at $\sim 3.5 \mu\text{m}$ below the apical PM were collected from double-labeled (Fig. 4, 1-P acceptor, donor and uFRET panels) and single-labeled (data not shown) images using 580-50 bandwidth emission filters. These images were then processed by the PFRET correction algorithm method¹² to generate the PFRET image (Fig. 4, 1-P PFRET panel), which shows the energy transfer levels. The acceptor (Fig. 4, 1-P acceptor panel), the quenched donor (Fig. 4, 1-P donor panel), and the PFRET (Fig. 4, 1-P PFRET panel) images are then used to calculate the three experimental parameters: acceptor, uD, and E% values (Figs. 7 and 8) used during data analysis. Comparing the uFRET and PFRET panels (Fig. 4, 1-P panels), it is clearly visible where contamination has been removed by treating the uFRET image with the PFRET algorithm.

A similar protocol is followed for 2-P microscopy with the exception that it only requires four images, including images of the single-label reference donor as well as double-labeled specimens with comparable fluorescence ranges taken under donor excitation wavelength with identical imaging conditions, since the acceptor Cy3 is not excited by the 790-nm

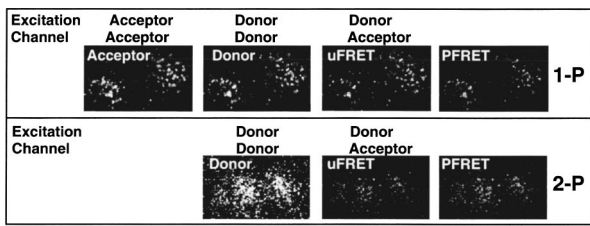


Fig. 4 1-P and 2-P imaging acceptor, donor, uFRET, and PFRET distributions of plgA-R-ligand complexes in apical endocytic membranes. Double-labeled MDCK polarized cells, containing co-internalized Alexa488- and Cy3-plgA-R-ligand complexes from opposite PM surfaces, were imaged by 1-P and 2-P microscopy at an xy (Z-section) focal plane $\sim 3.5 \mu\text{m}$ below the apical PM using 580-50 emission filter (wavelength range 555 to 605 nm). These images were modified in Adobe Photoshop at the same rate to a higher level of contrast for better visualization. Images shown (overall size $15 \times 7.5 \mu\text{m}$) contain two ROIs of similar size ($7.5 \times 7.5 \mu\text{m}$), each one containing a complete cell. Panel acceptor: acceptor excitation/acceptor channel shows acceptor fluorescence intensities (only in 1-P). Panel donor: donor excitation/donor channel shows the quenched donor fluorescence intensities. Panel uFRET: donor excitation/acceptor channel represents uFRET, which includes energy transfer levels plus the two contaminants in the FRET signal: donor crosstalk and acceptor bleed-through. Panel PFRET: uFRET image was processed by the PFRET algorithm, which removes donor crosstalk and acceptor bleed-through. The resulting image represents the actual energy transfer levels.

donor excitation wavelength.¹² As a precaution, we took an image of the single-label acceptor at the 790-nm donor excitation wavelength to confirm that there is no spillover into the FRET channel (data not shown). It is important to note that the 2-P uFRET image does not contain acceptor bleed-through contamination and thus only the donor crosstalk contamination is removed by treating the uFRET image with the PFRET algorithm. Consequently, the difference between the intensity of 2-P PFRET and uFRET images is reduced when compared to that of 1-P images.

The images in Fig. 4 contain two representative ROIs of similar size, each corresponding to one cell, which show the typical punctate pattern of apical endocytic membranes located at the level of the apical cytoplasm.

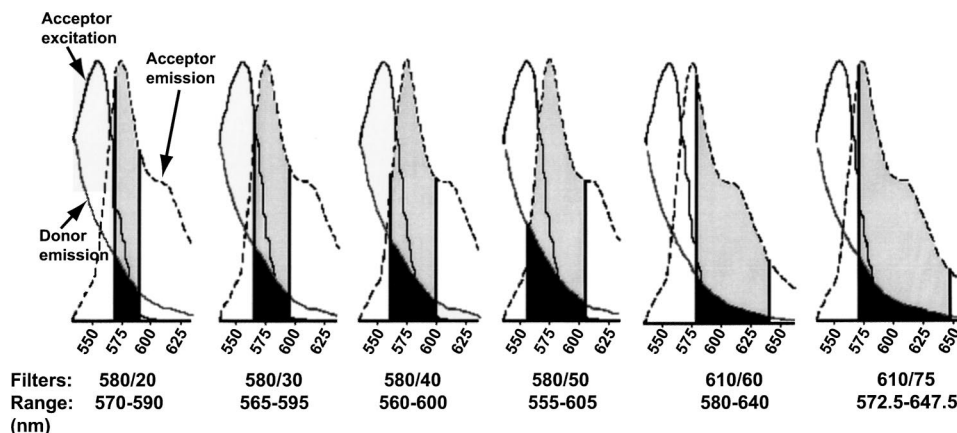


Fig. 5 Different emission filters with wider bandwidths lead to increased 1-P and 2-P FRET signals and corresponding spillover contamination. Six different emission filters: 580/20 (range 570 to 590 nm), 580/30 (range 565 to 595 nm), 580/40 (range 560 to 600 nm), 580/50 (range 555 to 605 nm), 610/60 (range 580 to 640 nm) and 610-75 (range 572.5 to 647.5 nm) were used to collect FRET images, which were then subjected to processing using PFRET correction algorithm.

3.3 FRET Analysis Using Emission Filters with Different Bandwidths and a FRET Spillover Algorithm-Based Correction Method

The establishment of a correct spectrogram is important for the selection of the emission filters, which in turn determines how much background fluorescence is collected, along with the FRET signal. Furthermore, it is critical to strike the right balance between reducing donor crosstalk and acceptor bleed-through FRET contamination and yet capture most of the FRET signal. FRET emission filters with different bandwidths allow different levels of FRET signals to be collected, however, with increasing FRET fluorescence the spillover contamination increases (Fig. 5).

We hypothesized that our algorithm-based correction method described earlier should demonstrate its utility by different levels of correction accompanied by comparable E% results. Our results support this assumption where wider bandwidths result in a higher percentage of correction (ANOVA p-value for 1-P=8.4E-18; 2-P=5.5E-14) while producing statistically indistinguishable E% values (ANOVA p-value for 1-P=0.19; 2-P=0.37) (Fig. 6). As expected, the average correction level is lower in 2-P than 1-P microscopy, due to the fact that we do not observe any acceptor bleed-through, as the donor wavelength does not excite the Cy3 fluorophore (acceptor).¹² We have no explanation for the higher than expected correction of the 580-20 filter in 2-P microscopy other than to point at the consistent E% figures, which are not affected by whatever caused the higher correction.

With the use of our correction algorithm, the choice of emission filter has now become less critical, both in 1-P and 2-P microscopy. For consistency, we continued to use the 590 LP filter in 1-P microscopy for the other experiments shown below. The 590LP filter catches the second of the two emission peaks of the acceptor Cy3 while at the same time limiting the background contamination. Based on our results, the second peak provides a strong enough signal to detect FRET (Figs. 3 and 4).

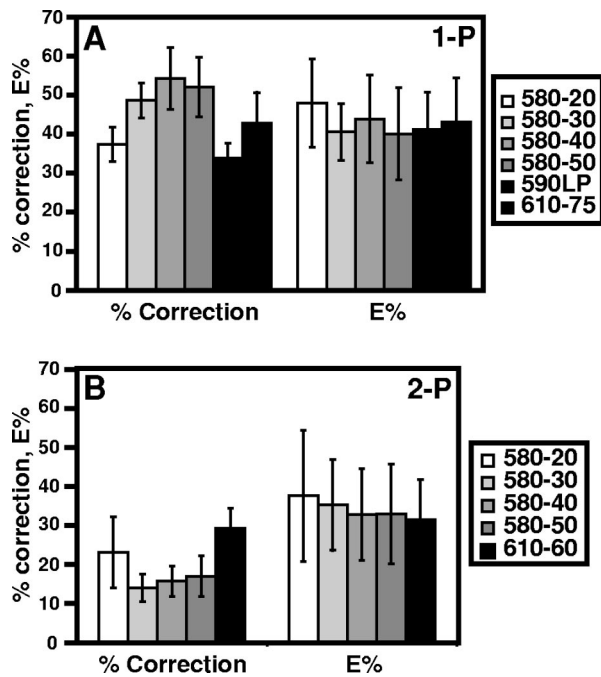


Fig. 6 PFRET correction levels increase with wider emission filter bandwidth, while resulting in comparable E% levels. Six different emission filters with wider bandwidth were used to test the PFRET correction analysis. PFRET correction levels (% correction) increase with the use of emission filters with wider bandwidth while E% values show comparable results. Correction levels are higher in 1-P than in 2-P since there is no acceptor bleed-through contamination of the FRET signal in 2-P. Nevertheless, comparable E% levels are obtained in 1-P and 2-P, thus validating our PFRET correction approach.

3.4 Negative Dependence of $uD:A$ Ratio and uD Levels on E% as an Indicator of Receptor Clustering Using 1-P and 2-P FRET Microscopy

Theories on how to distinguish between a clustered and a random distribution of membrane-bound proteins suggest that energy transfer between donor and acceptor molecules is governed by different dynamics with respect to E%, when the distribution is random or clustered.¹⁸⁻²⁰ E%'s independence from acceptor levels has been used as the main indicator for a clustered distribution pattern.¹⁸⁻²⁰ Our 1-P results indicate that E% is independent of the acceptor (data not shown). The phenomenon of decreasing E% with an increase in $uD:A$ ratio and uD levels can be used as another indicator of receptor clustering.¹⁸⁻²⁰ We call this donor geometric exclusion, where increasing the number of donor molecules within a cluster prevents other donors from being in FRET distance of an acceptor causing E% to decrease. We have developed a simplified model to describe our findings [Fig. 7(a)], where the share of total donor population rises, causing increasing steric hindrance. We have not included in our model the role of donor-donor competition and donor-donor energy transfer as contributing factors, which, while not appearing in the FRET channel, may nevertheless impact E%. As shown in Fig. 7(b), E% clearly decreases with increasing $uD:A$ ratio. Correlation analysis substantiates these conclusions, with values of $r = -0.77$, suggesting that clustering of receptor-ligand complexes occurs in apical endocytic membranes.

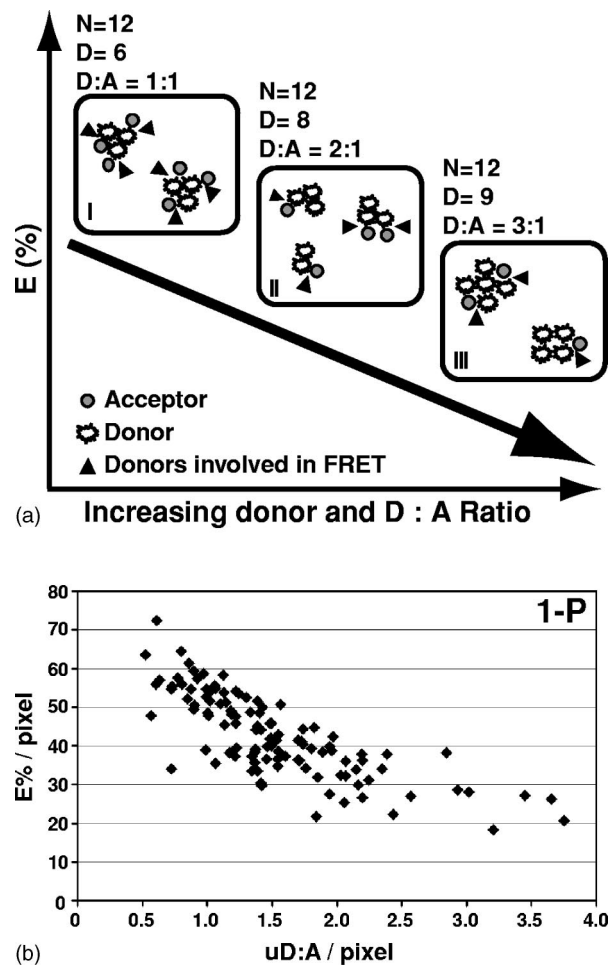


Fig. 7 (a) Donor geometric exclusion hypothesis. By definition, molecules in a cluster are in proximity. As the D:A ratio and/or the number of donor molecules increases, a phenomenon (donor geometric exclusion) occurs in which donors will block other donors from transferring energy to an acceptor due to increased steric hindrance, thus leading to a reduced E%. (b) Negative dependence of $uD:A$ ratio on E% using 1-P microscopy. E% was plotted against $uD:A$ ratios (Panel 1-P; diamonds). Qualitatively, the experimental results match the donor geometric exclusion hypothesis, confirming a clustered distribution.

When comparing 1-P and 2-P results, we see identical trends in the reduction of E% with increasing uD levels (Fig. 8). Correlation analysis confirms these conclusions, with values of $r = -0.72$ and $r = -0.85$, respectively, for 1-P and 2-P data. These results suggest that negative dependence of uD on E% can be used as an indicator of clustered distribution of receptor-ligand complexes in endocytic membranes. The relationship between uD levels and E% is especially useful for 2-P microscopy where we do not acquire acceptor data (Fig. 4), confirming a clustered distribution of receptor-ligand complexes.

4 Discussion

Specific membrane-bound proteins can either be assembled in clusters, distributed randomly, or possibly exhibit a continuum between these two states. Knowing the nature of molecular distribution will further our understanding of protein

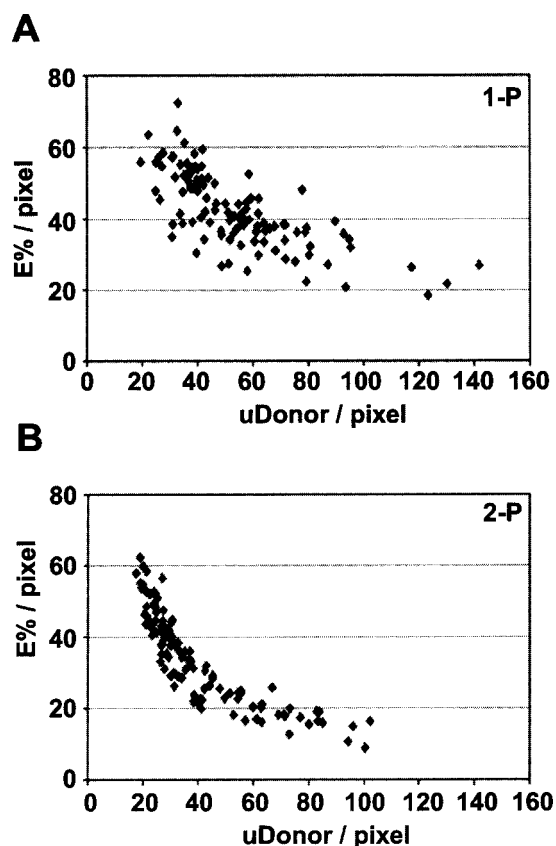


Fig. 8 Negative dependence of uD levels on E% is comparable using 1-P and 2-P FRET microscopy. E% was plotted against uD levels [(a) panel 1-P and (b) panel 2-P]. 1-P and 2-P microscopy, where we only collected donor information, show comparable results in which E% decreases when uD levels increase.

sorting and transport processes and endosomal organization. FRET—and in particular, energy transfer efficiency (E%)—is a most suitable method to explore such molecular associations, as the molecules have to be in close proximity for FRET to occur. The relationship of E% to acceptor fluorescence is a key indicator for random vs clustered distribution of membrane-bound proteins.^{18–20} Randomly distributed donors and acceptors increase their E% with increasing acceptor fluorescence, as the probability of an acceptor co-localizing with a potential donor for energy transfer increases. Conversely, in a clustered scenario where molecules by definition are in proximity, E% is largely independent of higher acceptor levels, as in a cluster with a choice of several acceptors at FRET distance, a donor can only transfer energy to one acceptor at a time. In a clustered distribution, D:A ratio has a negative dependence on E%, which can be regarded as a second indicator for receptor clustering.^{18–20} We propose that donor geometric exclusion, where donor molecules can prevent other donors from transferring energy to an acceptor molecule, explains the decrease of E% upon raising D:A ratio. Considering the donor geometric exclusion hypothesis, the negative dependency of uD levels on E% can also be used as an indicator of receptor clustering, which is particularly important for situations where acceptor values are not detected as in 2-P FRET microscopy.

4.1 PFRET Algorithm to Correct Spectral Spillover Contamination

Different spillover corrections methods exist—each perfectly suitable, depending on the level of sensitivity desired.^{7–11} For advanced quantitative evaluation, very sensitive methods, such as the recently developed PFRET algorithm, are essential.¹² The algorithm method was confirmed by the standard method of bleaching the acceptor (data not shown), where E% is calculated on the basis of donor emission before and after total photobleaching of the acceptor. Here, emission filters with different bandwidths were used, where increasing FRET fluorescence with filters of wider bandwidths caused increased spillover contamination. The PFRET algorithm corrects the spillover contamination at different levels of magnitude, accompanied by comparable and statistically indistinguishable E% results. While the type of emission filter may be less important with the new spillover correction algorithm, it is prudent to select filters that will collect optimal levels of the FRET signal, which in turn will lead to greater differentiation between data points. For our particular experimental system, the 590 LP emission filter is the most adequate to acquire high levels of FRET signal with a corresponding reduced spillover contamination.

4.2 Comparing 1-P with 2-P Microscopy

For our particular experimental system, both 1-P and 2-P microscopy produce comparable results. We are using a polarized epithelial MDCK cell line, where a monolayer of cells achieves a height of 15 to 20 μm . Imaging at a focal plane of $\approx 3.5 \mu\text{m}$ below the apical surface, the more discrete focal section achieved by 2-P microscopy does not appear to offer any advantages. For the determination of clustered distribution, the 2-P data analysis post-image acquisition only has to deal with donor crosstalk contamination, since the 790-nm donor excitation wavelength does not appear to excite the acceptor fluorophore¹² (data not shown). If acceptor information is required for specific experimental systems, a different excitation wavelength and/or donor-acceptor pair can be used. In summary, the FRET assay presented here is suitable to establish qualitatively and quantitatively whether clustering of membrane-bound complexes occurs in endocytic membranes.

Acknowledgments

We thank Chroma Technologies (Brattleboro, VT) for providing the different emission filters. We thank Heather M. Rowe and Dr. J.N. Demas (Department of Chemistry, University of Virginia) for their help in the spectral analysis of Cy3 and Alexa488 protein conjugates. We thank Jeff Larson of Nikon Inc. (Melville, NY) for his help with confocal microscopy. We thank Sarah Smith for her assistance with the experiments and data analysis. We thank the members of the Keck Center for Cellular Imaging, Dr. Lance Davidson (Department of Biology, University of Virginia), as well as members of the laboratories of Dr. Barroso and Dr. Bloom (Department of Biology, University of Virginia) for helpful discussions.

References

1. D. A. deAngelis, "Why FRET over genomics?," *Physiol. Genomics* **1**, 93–99 (1999).
2. P. I. H. Bastiaens and A. Squire, "Fluorescence lifetime imaging

- microscopy: spatial resolution of biochemical processes in the cell," *Trends Cell Biol.* **9**, 48–52 (1999).
3. J. R. Lakowicz, "Principles of fluorescence spectroscopy," 2nd Edition, Kluwer Academic/Plenum, New York (1999).
 4. P. Wu and L. Brand, "Resonance energy transfer: methods and applications," *Anal. Biochem.* **218**, 1–13 (1994).
 5. A. Periasamy, *Methods in Cellular Imaging*, p. 434, Oxford University Press, New York (2001).
 6. R. B. Sekar and A. Periasamy, "Fluorescence resonance energy transfer (FRET) microscopy imaging of live cell protein localizations," *J. Cell Biol.* **160**, 629–633 (2003).
 7. G. W. Gordon, G. Berry, X. H. Liang, B. Levine, and B. Herman, "Quantitative fluorescence resonance energy transfer measurements using fluorescence microscopy," *Biophys. J.* **74**, 2702–2713 (1998).
 8. P. I. Bastiaens and T. M. Jovin, "Microspectroscopic imaging tracks the intracellular processing of a signal transduction protein: fluorescent-labeled protein kinase C beta I," *Proc. Natl. Acad. Sci. U.S.A.* **93**, 8407–8412 (1996).
 9. F. S. Wouters, P. I. Bastiaens, K. W. Wirtz, and T. M. Jovin, "FRET microscopy demonstrates molecular association of non-specific lipid transfer protein (nsL-TP) with fatty acid oxidation enzymes in peroxisomes," *EMBO J.* **17**, 7179–7189 (1998).
 10. C. E. Chamberlain, V. S. Kraynov, and K. M. Hahn, "Imaging spatiotemporal dynamics of Rac activation *in vivo* with FLAIR," *Methods Enzymol.* **325**, 389–400 (2000).
 11. Z. Xia and Y. Liu, "Reliable and global measurement of fluorescence resonance energy transfer using fluorescence microscope," *Biophys. J.* **81**, 2395–2402 (2001).
 12. M. Elangovan, H. Wallrabe, R. N. Day, M. Barroso, and A. Periasamy, "Characterization of one- and two-photon fluorescence resonance energy transfer microscopy," *Methods* **29**, 58–73 (2003).
 13. M. Barroso and E. S. Sztul, "Basolateral to apical transcytosis in polarized cells is indirect and involves BFA and trimeric G protein sensitive passage through the apical endosome," *J. Cell Biol.* **124**, 83–100 (1994).
 14. P. S. Brown, E. Wang, B. Aroeti, S. J. Chapin, K. E. Mostov, and K. W. Dunn, "Definition of distinct compartments in polarized Madin-Darby canine kidney (MDCK) cells for membrane-volume sorting, polarized sorting and apical recycling," *Traffic* **1**, 124–140 (2000).
 15. A. Gibson, C. E. Futter, S. Maxwell, E. H. Allchin, M. Shipman, J.-P. Kraehenbuhl, D. Domingo, G. Odorizzi, I. S. Trowbridge, and C. R. Hopkins, "Sorting mechanisms regulating membrane protein traffic in the apical transcytotic pathway of polarized MDCK cells," *J. Cell Biol.* **143**, 81–94 (1998).
 16. S. C. D. van Ijzendoorn and D. Hoekstra, "The sub-apical compartment: a novel sorting center?," *Trends Cell Biol.* **9**, 144–149 (1999).
 17. W. Hunziker, P. Male, and I. Mellman, "Differential microtubule requirements for transcytosis in MDCK cells," *EMBO J.* **9**, 3515–3525 (1990).
 18. A. K. Kenworthy and M. Edidin, "Distribution of a glycosylphosphatidylinositol-anchored protein at the apical surface of MDCK cells examined at a resolution of 100 Å using imaging fluorescence resonance energy transfer," *J. Cell Biol.* **142**, 69–84 (1998).
 19. H. Wallrabe, M. Elangovan, A. Burchard, A. Periasamy, and M. Barroso, "Confocal FRET microscopy to measure clustering of ligand-receptor complexes in endocytic membranes," *Biophys. J.* **85**, 1–13 (2003).
 20. A. K. Kenworthy, N. Petranova, and M. Edidin, "High-resolution FRET microscopy of cholera toxin B-subunit and GPI-anchored proteins in cell plasma membranes," *Mol. Biol. Cell.* **11**, 1645–1655 (2000).